Development of Functional Scaffolds for Bone Tissue Engineering using 3D-bioprinting of Cells and Biomaterials

Zamani, Y.

2020

document version
Publisher's PDF, also known as Version of record

CHAPTER 5

Bioprinting of Alginate-Encapsulated MC3T3-E1 Pre-osteoblasts in PLGA/β-TCP Scaffolds Enhances Cell Retention but Impairs Cell Proliferation and Osteogenic Differentiation Compared to Cell-Seeding after 3D-Printing

Yasaman Zamani[1,2], Javad Mohammadi[1], Ghassem Amoabediny[2,3,4], Marco N. Helder[4], Behrouz Zandieh-Doulabi[5], Jenneke Klein-Nulend[5]

[1] Department of Biomedical Engineering, Faculty of New Sciences and Technologies, University of Tehran, Tehran, Iran

[2] Department of Biomedical Engineering, Research Center for New Technologies in Life Science Engineering, University of Tehran, Tehran, Iran

[3] School of Chemical Engineering, College of Engineering, University of Tehran, Tehran, Iran

[4] Department of Oral and Maxillofacial Surgery/Oral Pathology, Amsterdam University Medical Centers-location VUmc and Academic Centre for Dentistry Amsterdam (ACTA), Amsterdam Movement Sciences, Amsterdam, the Netherlands

[5] Department of Oral Cell Biology, Academic Centre for Dentistry Amsterdam (ACTA)-University of Amsterdam and Vrije Universiteit Amsterdam, Amsterdam Movement Sciences, Amsterdam, The Netherlands

Submitted for publication

ABSTRACT

Tissue engineering, relying on the combination of scaffolds, cells, and biological molecules has developed as a promising strategy for treatment of bone defects. Cellularization of scaffolds has typically been performed by seeding the cells after scaffold fabrication. Additive manufacturing technology and in particular 3D-printing, now allows bioprinting of cells encapsulated in a hydrogel simultaneously with the scaffold material. Here, we aimed to investigate whether bioprinting or cell seeding post-printing is more effective in enhancing cell seeding efficiency, pre-osteoblasts proliferation and differentiation. We incorporated MC3T3-E1 pre-osteoblasts in poly(lactic-co-glycolic acid)/β-tricalcium phosphate (PLGA/β-TCP) scaffolds by either seeding the cells after scaffold printing, or by bioprinting alginate-encapsulated cells layer-by-layer between the PLGA/β-TCP struts, and investigated whether differences existed in pre-osteoblasts responses. Cell retention was 51 ± 5% in cell-seeded and 87 ± 3% in bioprinted scaffolds, whereas cell viabilities were 87 ± 2% and 78 ± 4%, respectively. Cell proliferation was higher on cell-seeded scaffolds (day 7: 2.5-fold, day 14: 4.0-fold, day 21: 4.7-fold) compared with bioprinted scaffolds (1.2-fold, 2.1-fold, and 3.9-fold, respectively). After 21 days of culture, the voids between the PLGA/β-TCP struts were covered with cell-deposited collagenous matrix in both scaffold types. Alkaline phosphatase activity was significantly higher (3.4-fold) on cell-seeded scaffolds compared with bioprinted scaffolds. Our data demonstrate that encapsulation of MC3T3-E1 pre-osteoblasts in alginate and printing inside PLGA/β-TCP scaffolds enhances cell retention but decreases cell proliferation and osteogenic differentiation compared to seeding the cells on the scaffolds post-printing. This might have important implications for bone tissue engineering.

Keywords
Alginate, bioprinting, cell retention, osteogenic differentiation, PLGA/β-TCP, pre-osteoblasts

INTRODUCTION

Bone defects are among the most common injuries in the body due to aging population, metabolic diseases such as osteoporosis, infectious diseases, and cancer. Bone is known for its self-healing capacity; however, 5-10% of bone defects end in nonunion and/or incomplete healing [1]. Although autografts are considered the standard treatment for nonunions, they have certain limitations such as limited supply, need for multiple surgeries, and possibility of damage to the nerves [2]. Bone tissue engineering is a promising alternative, eliminating the need for additional surgeries and donor site morbidity. The aim of tissue engineering is to replace, maintain, or enhance the function of damaged or diseased tissues by a combination of scaffolds, cells, and biological molecules [3]. A porous scaffold is crucial to provide a microenvironment for cell activities. The most commonly used materials for fabrication of bone tissue engineering scaffolds are calcium phosphates such as hydroxyapatite and β-tricalcium phosphate (β-TCP), poly(α-hydroxy esters) such as poly(ε-caprolactone) (PCL), polylactic acid (PLA), and poly(lactic-co-glycolic) acid (PLGA), and their composites [4, 5]. The main advantage of these polymers is their tailorable degradation rate and the removal of their degradation products by natural processes without adverse effects [6]. These polymers also have suitable mechanical properties for bone replacement, and are approved by the US Food and Drug Administration [7]. PLGA is the most popular biodegradable polymer due to its outstanding advantages including suitable mechanical properties especially toughness, adjustability of degradation rate, and excellent processability [8]. However, PLGA itself lacks osteoinductivity [9]. Therefore, materials enhancing bone formation such as hydroxyapatite and β-TCP are extensively used as a composite with PLGA [10-12].

Bone tissue engineering scaffolds have traditionally been fabricated using techniques such as freeze drying, solvent casting-porogen leaching, and gas foaming. These fabrication methods have limitations such as toxic solvent residues, inaccurate control of internal structure, and poor ability to customize for specific defect sites [13]. Additive manufacturing (AM) is a relatively new technology in which the final structure is built by adding layers of material based on a computer aided-design (CAD) file. AM technologies have attracted the attention of many fields especially the medical industry. One of the medical applications of AM is fabrication of tissue engineering scaffolds. In this regard, techniques such as fused deposition modeling (FDM), selective laser sintering (SLS), powder-based and extrusion-based 3D-printing are used for fabrication of scaffolds with controlled internal structure and geometry according to the defect site, whereafter target cells are seeded on the scaffolds [14]. However, conventional cell seeding methods have limitations such as low seeding efficiency and inhomogeneous distribution of cells

within the scaffold [15]. With the further development of 3D-printing technologies, it is now possible to print cells simultaneously with the scaffold material referred to as “3D-bioprinting”. 3D-bioprinting has several advantages such as homogeneous distribution of cells in the scaffold and the ability to print several cell types at pre-defined locations in a single scaffold [16]. In order to prevent damage to the cells in the process of printing, cells need to be encapsulated in a hydrogel. Hydrogels are 3D networks that have a high water content. Several hydrogels such as fibrin [17], agarose [18], alginate [19], and gelatin methacrylate (GelMA) [20] have been used for cell printing. Alginate is a biocompatible natural polysaccharide composed of guluronic and mannuronic acids [21]. Due to its biodegradability, low cost, and gelation under mild conditions, alginate has been frequently used for encapsulation of cells in the bioprinting of bone tissue engineering scaffolds [22-25]. When cells are encapsulated in a hydrogel, some cell functions might be affected by the hydrogel properties [26]. Moreover, during the bioprinting process, cells might experience unintended shear stress that may affect their function [27]. Whether bioprinting in alginate or cell seeding post-printing is more effective to enhance pre-osteoblast proliferation and differentiation is currently unknown. In the present study, we incorporated MC3T3-E1 pre-osteoblasts in PLGA/β-TCP scaffolds by either seeding strategy, using alginate as the hydrogel carrier, and investigated whether differences exist in the response of pre-osteoblasts to these two scaffold types.

MATERIALS AND METHODS

Preparation of PLGA/β-TCP pellets

Medical grade PLGA granules (Purasorb, Purac Biomaterials, Netherlands) were melted on a hot plate at 100°C. β-TCP (particle size: 0.5-1 μm, Nik Ceram Razi, Isfahan, Iran) was added to the molten PLGA in a 25 wt% ratio, and was homogenized for 1 h to homogeneously disperse the β-TCP particles in the PLGA. Upon removal from the hot plate, PLGA/β-TCP pellets were obtained.

3D-printing of PLGA/β-TCP scaffolds

Scaffolds were designed using BioCAD^{TM} software (RegenHU, Villaz-St-Pierre, Switzerland). PLGA/β-TCP pellets were melted at 110°C in the heating tank of the 3D Discovery bioprinter (RegenHU) and extruded through a pre-heated needle at 0.4 MPa (4 Bar). The struts of PLGA/β-TCP were plotted layer-by-layer on the platform until the desired height was achieved. Cubical scaffolds with dimensions of 10×10×5 mm were fabricated.

MC3T3-E1 pre-osteoblasts seeding on the 3D-printed PLGA/β-TCP scaffolds

MC3T3-E1 pre-osteoblasts were obtained from the American Type Culture Collection (ATCC, Manassas, VA, USA). Cells were grown and maintained in α-Minimum Essential Medium (α-MEM; Gibco, Life Technologies, Waltham, MA, USA) supplemented with 10% fetal bovine serum (FBS; BioWest SAS, Nuaille, France) and 1% PSF (antibiotic antimycotic solution, Sigma-Aldrich®, St. Louis, MO, USA) in a humidified incubator with 5% CO_2 in air at 37°C. After reaching ~75% confluency, cells were detached using 0.25% trypsin (Gibco, Invitrogen, Waltham, MA, USA) and 0.1% ethylenediaminetetraacetic acid (Merck, Darmstadt, Germany) in phosphate-buffered saline (PBS) at 37°C. Cells were then re-suspended in α-MEM with 10% FBS, 1% PSF, 50 µg/ml ascorbic acid, and 10 mM β-glycerophosphate (osteogenic medium) and seeded on the scaffolds at a density of 5×10^5 cells/cm^3 scaffold and incubated in a humidified incubator with 5% CO_2 in air at 37°C.

MC3T3-E1 pre-osteoblasts encapsulation in alginate

Sodium alginate powder (Sigma-Aldrich) was sterilized under UV for 20 min and dissolved in culture medium. The alginate solution was vortexed at high speed and subsequently kept at room temperature for at least 1 h to minimize bubbles in the solution. To encapsulate cells in alginate, cultured pre-osteoblasts were slowly suspended at a density of 4×10^6 cells/ml in 6 wt% alginate solution and transferred into a 10 ml sterile syringe. Every 0.5 ml of this cell suspension was used to print 4 scaffolds and therefore, 5×10^5 cells were printed in each scaffold.

3D-bioprinting of MC3T3-E1 pre-osteoblasts in PLGA/β-TCP scaffolds

Scaffolds were designed using BioCAD™ software (RegenHU, Villaz-St-Pierre, Switzerland). PLGA/β-TCP pellets were melted at 110°C in the heating tank and extruded through the pre-heated thermoplastic polymer nozzle at 0.4 MPa (4 Bar). In the first layer, PLGA/β-TCP struts were deposited in parallel and then, cells encapsulated in alginate were deposited between the PLGA/β-TCP struts by passing through a 21-gauge (21G) needle. The subsequent layers were deposited with the same pattern but with a deposition angle of 90° until the required height was obtained. When the structure was complete, scaffolds were immersed in 102 mM $CaCl_2$ for 10 min to crosslink the alginate. Afterwards, osteogenic medium was added to the scaffolds in 24-well culture plates. Scaffolds were incubated in a humidified incubator with 5% CO_2 in air at 37°C. The fabrication process of the cell-seeded and the bioprinted scaffolds is schematically illustrated in figure 1.

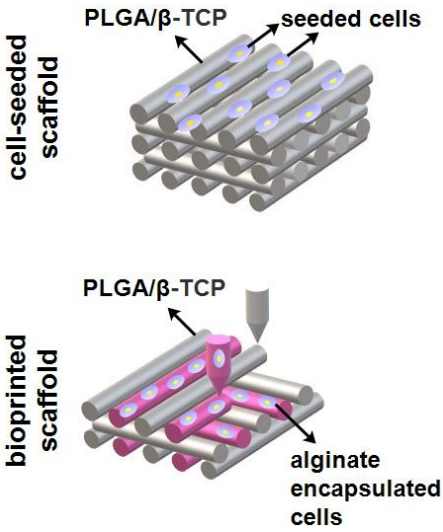

Figure 1. Schematic illustration of the cell seeding post-printing and the bioprinting process. In the first approach, the scaffold consisting of PLGA/β-TCP struts was printed layer by layer and then MC3T3-E1 pre-osteoblasts were seeded onto the scaffold. In the second approach, MC3T3-E1 pre-osteoblasts were encapsulated in alginate and were printed simultaneously between PLGA/β-TCP struts.

MC3T3-E1 pre-osteoblasts retention

Sixteen hours after cell seeding and cell printing, cell/scaffold constructs in a 24-well culture plate ("old plate") were washed twice with PBS, and transferred to a new 24-well culture plate. Cell retention was assessed by determining the number of cells attached to the wells of the old plate as well as the number of cells attached to the scaffolds, using AlamarBlue® fluorescent assay (Invitrogen, Frederick, MD, USA), according to the manufacturer's instructions. We found a linear relationship between AlamarBlue® fluorescence and cell number (data not shown). Ten percent AlamarBlue® solution in fresh osteogenic medium was added to the wells of the old plate and to each scaffold until it completely covered the top of the scaffolds. Scaffolds and old plate were incubated in AlamarBlue® solution for 4 h in a humidified incubator with 5% CO_2 at 37°C. The solution was harvested from the scaffolds and the old plate, and the fluorescence was measured at 530 nm with a Synergy HT® spectrophotometer. Scaffolds were washed twice with PBS, and incubated in a humidified incubator with 5% CO_2 at 37°C. Cell retention was calculated according to the following equation [28]:

$$\text{Cell retention (\%)} = \frac{\text{number of cells attached to the scaffold}}{\text{number of cells attached to the scaffold + number of cells attached to the plate}} \times 100$$

Scaffolds were assayed in triplicate.

MC3T3-E1 pre-osteoblasts viability

A live/dead viability/cytotoxicity kit (L3224; Thermo Fisher Scientific, Waltham, MA, USA) was used to assess cell viability in the cell-seeded and the bioprinted scaffolds according to manufacturer's instructions. Briefly, 16 h post cell seeding and cell printing, cell/scaffold constructs were washed in PBS, followed by incubation in 0.5 µl/ml calcein acetoxymetyl (Cal-AM) and 2 µl/ml ethidium homodimer-1 (EthD) in PBS at 37°C for 1.5 h. Concentration of Cal-AM and EthD stock solutions was 4 mM in anhydrous dimethyl sulfoxide (DMSO) and 2 mM in DMSO/H_2O 1:4 (v/v), respectively. Cell/scaffold constructs were washed again in PBS and imaged using fluorescent microscopy (Leica Microsystems, Wetzlar, Germany). Live and dead cell quantification was performed in ImageJ v1.8 for windows.

MC3T3-E1 pre-osteoblasts proliferation

Proliferation was assessed by determining cell number in scaffolds at days 1, 7, 14, and 21, and by dividing these numbers to cell number in the scaffolds at day 1 using AlamarBlue® fluorescent assay, as described above under "cell retention". At each time point, scaffolds were transferred to a new plate, AlamarBlue® was added to the scaffolds, and fluorescence was measured. Thereby, cells attached to the old plates were not included in the measurements. After performing the AlamarBlue® assay at each time point, scaffolds were washed twice with PBS, and incubated in osteogenic medium in a humidified incubator with 5% CO_2 at 37°C. Scaffolds were assayed in triplicate.

Collagenous matrix deposition by MC3T3-E1 pre-osteoblasts

Picrosirius red stain kit (Chondrex, Inc., Redmond, WA, USA) was used to visualize collagen deposition on the scaffolds. After 21 days of culture, cell/scaffold constructs were washed thoroughly with PBS and fixed in 4% formaldehyde. Fixed constructs were stained for 2 h with picrosirius red at room temperature. Then, constructs were washed twice with acidified water (5 ml acetic acid/L distilled water) and visualized using a Leica inverted microscope (Leica Microsystems, Wetzlar, Germany).

Alkaline phosphatase activity and protein assay

Alkaline phosphate (ALP) activity was measured to assess the osteoblastic phenotype of MC3T3-E1 pre-osteoblasts in the cell-seeded and the bioprinted PLGA/β-TCP scaffolds. At day 21 of cell culture on the scaffolds, cell/scaffold constructs were subjected to cell lysis. Cells were lysed with the CyQuant® lysis buffer (Molecular Probes/Invitrogen, Carlsbad, CA, USA) and freeze-thawed

3 times to determine ALP activity and protein content. P-nitrophenyl-phosphate (Merck, Darmstadt, Germany) at pH 10.3 was used as substrate for ALP as described earlier [29]. The absorbance was read at 410 nm. ALP activity was expressed as μM/μg cellular protein. The amount of protein was determined by using a BCA Protein Assay reagent Kit (Pierce™, Rockford, Ill, USA), and the absorbance was read at 540 nm with a Synergy HT® spectrophotometer. ALP activity was also stained and visualized using nitro blue tetrazolium chloride/5-bromo-4-chloro-3-indolyl phosphate (NBT/BCIP; Roche, Germany) following the standard protocols. Constructs were assayed in triplicate.

Statistical analysis

Data are expressed as mean ± standard deviation (SD). Differences in mean values were analyzed by unpaired two-tailed t test using GraphPad Prism® 7.0 (GraphPad Software Inc., La Jolla, CA, USA). Differences were considered significant if $p<0.05$.

RESULTS

MC3T3-E1 pre-osteoblasts retention in cell-seeded and bioprinted PLGA/β-TCP scaffolds

Cell retention, which is expressed as the percentage of cells attached to the scaffold to the total number of cells initially incorporated in the scaffolds, was measured 16 h after seeding and printing. Cell retention was 1.7-fold higher in the bioprinted scaffold (87 ± 3%) compared with the cell-seeded scaffold (51 ± 5%; Fig. 2a).

MC3T3-E1 pre-osteoblasts viability in cell-seeded and bioprinted PLGA/β-TCP scaffolds

Cell viability was measured 16 h after seeding and printing using live/dead staining. Cell viability was higher by 1.1-fold in the cell-seeded scaffold (87 ± 2%) compared with the bioprinted scaffold (78 ± 4%; Fig. 2b). Live cells appeared as green dots and dead cells appeared as red dots in the fluorescent microscopy images (Fig. 2c). Lower cellular density was observed on the cell-seeded scaffold compared with the bioprinted scaffold by visual inspection.

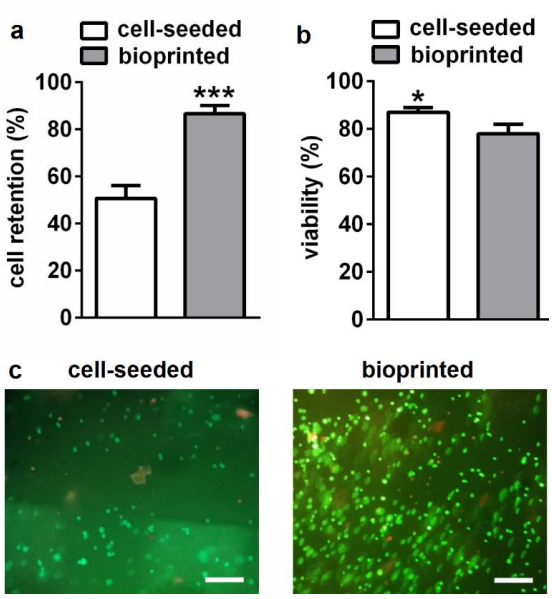

Figure 2. Cell retention and viability in cell-seeded and bioprinted PLGA/β-TCP scaffolds. (a) Cell retention was measured 16 h after seeding and printing. Cell retention was 51 ± 5% in the cell-seeded and 87 ± 3% in the bioprinted scaffold. (b) Cell viability was measured using live/dead staining images 16 h after seeding and printing. Cell viability was 87 ± 2% in the cell-seeded and 78 ± 4% in the bioprinted scaffold. (c) Live/dead staining images of cell-seeded and bioprinted PLGA/β-TCP scaffolds. Lower cellular density was observed in the cell-seeded scaffold compared with the bioprinted scaffold. Scale bar, 200 µm. Green dots, live cells; red dots, dead cells. Values are mean ± SD (n=3). *Significantly different from the other group, $p<0.05$, ***$p<0.001$.

MC3T3-E1 pre-osteoblasts proliferation and collagenous matrix deposition in cell-seeded and bioprinted PLGA/β-TCP scaffolds

Cell proliferation in cell-seeded and bioprinted PLGA/β-TCP scaffolds was assessed after 7, 14, and 21 days of culture, and compared relative to day 1 (Fig. 3a). Cell proliferation was higher in the cell-seeded scaffold (day 7: 2.5-fold, day 14: 4.0-fold, day 21: 4.7-fold) compared with the bioprinted scaffold (day 7: 1.2-fold, day 14: 2.1-fold, day 21: 3.9-fold). The difference in cell proliferation between the two scaffold types was more pronounced at day 14 and reduced at day 21. After 21 days of culture, the voids between the PLGA/β-TCP struts were covered to the same extent with cell-deposited collagenous matrix in both cell-seeded and bioprinted scaffolds (Fig. 3b).

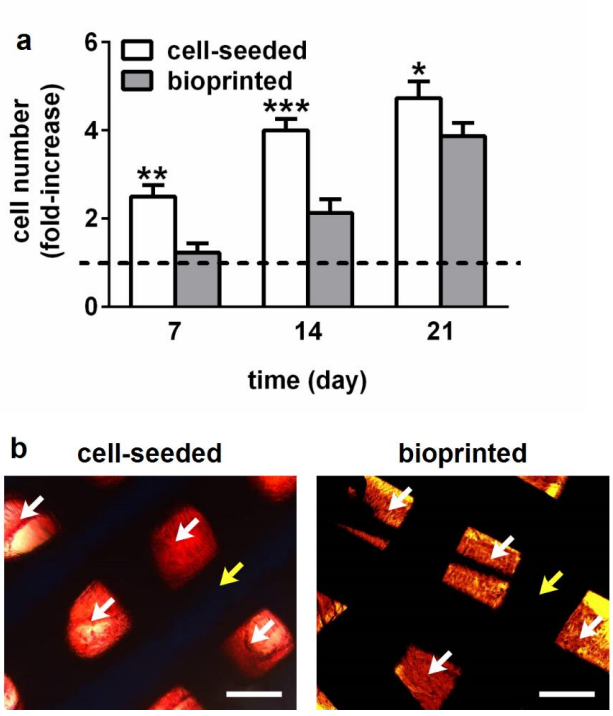

Figure 3. MC3T3-E1 pre-osteoblasts proliferation and collagenous matrix deposition in cell-seeded and bioprinted PLGA/β-TCP scaffolds. (a) MC3T3-E1 pre-osteoblasts proliferation in scaffolds was measured after 7, 14, and 21 days of culture, and compared relative to day 1. At all time points, proliferation was higher in the cell-seeded compared with the bioprinted PLGA/β-TCP scaffolds. The difference in proliferation rate between the two scaffolds was more pronounced at day 14 and reduced at day 21. (b) After 21 days of culture, the voids between the PLGA/β-TCP struts were covered with cell-deposited collagenous matrix on both scaffold types. Scale bar, 300 μm. Yellow arrows, PLGA/β-TCP struts; white arrows, collagen. Values are mean ± SD (n=3). *Significantly different from the other group, $p<0.05$, **$p<0.01$, ***$p<0.001$.

ALP activity by MC3T3-E1 pre-osteoblasts in cell-seeded and bioprinted PLGA/β-TCP scaffolds

ALP activity of MC3T3-E1 pre-osteoblasts in cell-seeded and bioprinted PLGA/β-TCP scaffolds was measured at day 21 and normalized to total protein content. ALP activity was significantly higher (3.4-fold) in the cell-seeded scaffold compared with the bioprinted scaffold (Fig. 4a). In the ALP stained images, more purple areas representing higher ALP activity and osteogenic differentiation was observed in the cell-seeded scaffold compared with the bioprinted scaffold (Fig. 4b).

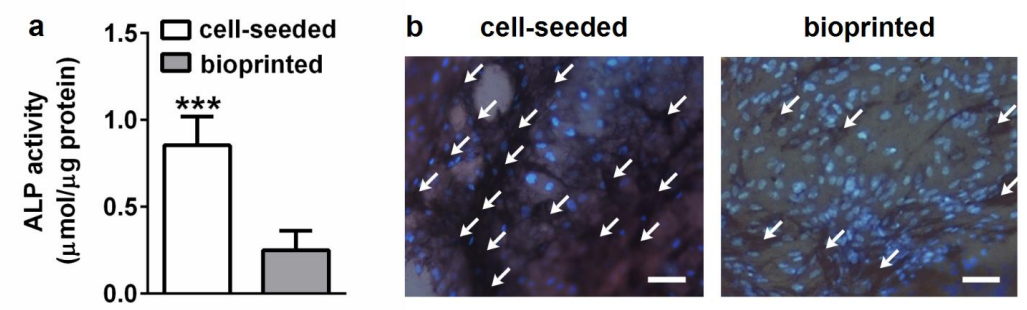

Figure 4. ALP activity and staining in cell-seeded and bioprinted PLGA/β-TCP scaffolds. (a) ALP activity was significantly higher in the cell-seeded scaffold compared with the bioprinted scaffold. (b) More purple areas representing higher ALP activity and osteogenic differentiation was observed in the cell-seeded scaffold compared with the bioprinted scaffold. Scale bar, 100 µm. Blue dots, cell nuclei; white arrows, areas with ALP activity. Values are mean ± SD (n=3). ***Significantly different from the other group, $p<0.001$.

DISCUSSION

Conventional cell seeding methods have limitations such as low seeding efficiencies and inhomogeneous distribution of cells inside the scaffold [15]. With the development of bioprinting technology, it is now possible to print cells inside the scaffold during layer-by-layer scaffold fabrication. This technology has several advantages such as homogeneous distribution of cells in the scaffold and the ability to print several cell types at pre-defined locations in a single scaffold [16]. Nevertheless, bioprinting has certain disadvantages compared to traditional cell seeding approaches including that during bioprinting, cells are exposed to certain types of stress that might adversely affect their function [27]. We incorporated MC3T3-E1 pre-osteoblasts in PLGA/β-TCP scaffolds by either seeding the cells post scaffold printing or by bioprinting the cells encapsulated in alginate layer-by-layer between the PLGA/β-TCP struts and investigated whether differences exist in the response of pre-osteoblasts to these two scaffold types. We found that (i) cell retention was lower in the cell-seeded compared to the bioprinted PLGA/β-TCP scaffolds, (ii) cell viability was slightly higher in the cell-seeded compared to the bioprinted PLGA/β-TCP scaffolds, (iii) cell proliferation was higher in the cell-seeded compared to the bioprinted PLGA/β-TCP scaffolds, (iv) the voids between the PLGA/β-TCP struts were covered with cell-deposited collagenous matrix on both scaffold types, and (v) ALP activity was higher in the cell-seeded compared to the bioprinted PLGA/β-TCP scaffolds.

Cell retention refers to the ratio of cells that remained in the scaffold after cell incorporation, to the total number of cells seeded on or printed in the scaffold. Cell retention was lower in the cell-seeded scaffold compared with the bioprinted scaffold. When cells are seeded on a 3D-printed scaffold, a fraction of cells go through the scaffold voids and adhere to the plate instead of attaching to the scaffold struts. The percentage of cell attachment to the scaffold depends on several factors such as scaffold surface hydrophilicity and roughness [30, 31]. On the other hand, when cells are encapsulated in a hydrogel and deposited layer-by-layer between the scaffold struts, it is more difficult for cells to leave the scaffold and attach to the plate. Therefore, a higher percentage of cells remain in the scaffold. The live/dead staining images confirmed these results as lower cellular density was observed in the cell-seeded scaffold compared to the bioprinted scaffold.

Cell viability which is the ratio of live cells to the entire cells in the scaffold was slightly higher in the cell-seeded scaffold (87 ± 2%) compared with the bioprinted scaffold (78 ± 4%). This might be due to the harsh conditions that cells undergo during printing. In the process of cell printing, different parameters such as extrusion pressure, needle diameter, needle height, and needle head speed affect cell viability [32]. The extrusion pressure has been shown to have the most significant effect due to the exposed shear stress on the cells [33]. On the contrary, cells do not experience such harsh conditions when seeded on the scaffold which could be the reason for higher cell viability on the cell-seeded scaffold compared with the bioprinted scaffold. These findings are in agreement with data by others who showed that despite high cellular density in the bioprinted scaffold, cell viability is reduced due to the shear stress [32].

Proliferation of MC3T3-E1 pre-osteoblasts was higher in the cell-seeded scaffold compared with the bioprinted PLGA/β-TCP scaffold. This is probably due to encapsulation of cells in the alginate in the bioprinting process. Although alginate is known to be a suitable hydrogel for encapsulation of cells and can act as a template to permit cell localization [22], it is a relatively biologically inert material and provides cells with a non-interactive encapsulation matrix [34, 35]. This results in weaker interaction between the cells that is essential for cellular functions such as proliferation and differentiation [36]. Nevertheless, cells could deposit collagenous matrix in both scaffolds by day 21, i.e. in both scaffolds, the voids between the PLGA/β-TCP struts were filled with collagenous matrix indicating the presence of viable functioning cells in both scaffold types by day 21.

We found higher ALP activity, indicating enhanced osteogenic differentiation in the cell-seeded scaffold compared with the bioprinted scaffold. Cell-material interaction is a key factor for cell survival and determines the majority of cellular functions such as cell migration, proliferation,

differentiation, and death [37]. When seeded on the PLGA/β-TCP scaffold, cells were in direct contact with the surface of the PLGA/β-TCP struts. This was advantageous for osteogenic differentiation since PLGA/β-TCP struts have a hydrophilic surface with suitable surface roughness required for osteogenic differentiation. Moreover, β-TCP particles can help induce osteogenic differentiation of the pre-osteoblasts [38]. However, when cells were encapsulated in alginate, interaction of cells with the surface of the PLGA/β-TCP struts was hampered by the alginate layer. Rather, cells were dispersed in a soft non-osteoinductive matrix which resulted in lower osteogenic differentiation of the pre-osteoblasts. Our results are in agreement with data by others who showed that alginate encapsulation parameters influence the differentiation of the encapsulated cells [39, 40]. We postulate that incorporation of bioactive molecules in the alginate formulation might enhance the osteogenic potential of alginate-based bioprinted scaffolds.

CONCLUSION

In conclusion, the bioprinted scaffolds had enhanced cell retention, but impaired cell proliferation and osteogenic differentiation compared to the cell-seeded scaffolds. This might have important implications for the improvement of alginate-based bioinks with e.g. (natural) bioactive peptides for bioprinting of bone tissue engineering scaffolds.

REFERENCES

1. Buza III JA, Einhorn T. Bone healing in 2016. Clin Cases Miner Bone Metab 2016;13:101-105.
2. Marino JT, Ziran BH. Use of solid and cancellous autologous bone graft for fractures and nonunions. Orthop Clin North Am 2010;41:15-26.
3. Nerem RM. Regenerative medicine: the emergence of an industry. J R Soc Interface 2010;7:S771-S775.
4. Arul KT, Manikandan E, Ladchumananandasivam R. Polymer-based calcium phosphate scaffolds for tissue engineering applications. In: Grumezescu AM (ed) Nanoarchitectonics in Biomedicine, William Andrew Publishing 2019:585-618.
5. Ramesh N, Moratti SC, Dias GJ. Hydroxyapatite-polymer biocomposites for bone regeneration: a review of current trends. J Biomed Mater Res B App Biomater 2018;106:2046-2057.
6. Yu NY, Schindeler A, Little DG, Ruys AJ. Biodegradable poly (α-hydroxy acid) polymer scaffolds for bone tissue engineering. J Biomed Mater Res B App Biomater 2010;93:285-295.
7. Felfel R, Poocza L, Gimeno-Fabra M, Milde T, Hildebrand G, Ahmed I, Scotchford C, Sottile V, Grant DM, Liefeith K. In vitro degradation and mechanical properties of PLA-PCL copolymer unit cell scaffolds generated by two-photon polymerization. Biomed Mater 2016;11:015011.
8. Pan Z, Ding J. Poly(lactide-co-glycolide) porous scaffolds for tissue engineering and regenerative medicine. Interface Focus 2012;2:366-377.
9. Sun X, Xu C, Wu G, Ye Q, Wang C. Poly(lactic-co-glycolic acid): applications and future prospects for periodontal tissue regeneration. Polymers (Basel) 2017;9:189.
10. Yoshida T, Miyaji H, Otani K, Inoue K, Nakane K, Nishimura H, Ibara A, Shimada A, Ogawa K, Nishida E, Sugaya T, Sun L, Fugetsu B, Kawanami M. Bone augmentation using a highly porous PLGA/β-TCP scaffold containing fibroblast growth factor-2. J Periodontal Res 2015;50:265-273.
11. Bizenjima T, Takeuchi T, Seshima F, Saito A. Effect of poly (lactide-co-glycolide) (PLGA)-coated beta-tricalcium phosphate on the healing of rat calvarial bone defects: a comparative study with pure-phase beta-tricalcium phosphate. Clin Oral Implants Res 2016;27:1360-1367.
12. Lee SK, Han CM, Park W, Kim IH, Joung YK, Han DK. Synergistically enhanced osteoconductivity and anti-inflammation of PLGA/β-TCP/$Mg(OH)_2$ composite for orthopedic applications. Mater Sci Eng C Mater Biol Appl 2019;94:65-75.
13. Roseti L, Parisi V, Petretta M, Cavallo C, Desando G, Bartolotti I, Grigolo B. Scaffolds for bone tissue engineering: state of the art and new perspectives. Mater Sci Eng C 2017;78:1246-1262.
14. Miar S, Shafiee A, Guda T, Narayan R. Additive manufacturing for tissue engineering. In: Ovsianikov A, Yoo J, Mironov V (eds) 3D Printing and Biofabrication. Reference Series in Biomedical Engineering. Springer, Cham. 2018:3-54.
15. Chan BP, Leong KW. Scaffolding in tissue engineering: general approaches and tissue-specific considerations. Eur Spine J 2008;17:467-479.

16. Piard CM, Chen Y, Fisher JP. Cell-laden 3D printed scaffolds for bone tissue engineering. Clinic Rev Bone Miner Metab 2015;13:245-255.
17. England S, Rajaram A, Schreyer DJ, Chen X. Bioprinted fibrin-factor XIII-hyaluronate hydrogel scaffolds with encapsulated Schwann cells and their in vitro characterization for use in nerve regeneration. Bioprinting 2017;5:1-9.
18. Duarte CD, Blaeser A, Weber M, Jäkel J, Neuss S, Jahnen-Dechent W, Fischer H. Three-dimensional printing of stem cell-laden hydrogels submerged in a hydrophobic high-density fluid. Biofabrication 2013;5:015003.
19. Tabriz AG, Hermida MA, Leslie NR, Shu W. Three-dimensional bioprinting of complex cell laden alginate hydrogel structures. Biofabrication 2015;7:045012.
20. Pepelanova I, Kruppa K, Scheper T, Lavrentieva A. Gelatin-methacryloyl (GelMA) hydrogels with defined degree of functionalization as a versatile toolkit for 3D cell culture and extrusion bioprinting. Bioengineering (Basel) 2018;5:55.
21. Pawar SN, Edgar KJ. Alginate derivatization: a review of chemistry, properties and applications. Biomaterials 2012;33:3279-3305.
22. Axpe E, Oyen M. Applications of alginate-based bioinks in 3D bioprinting. Int J Mol Sci 2016;17:1976.
23. Bendtsen ST, Quinnell SP, Wei M. Development of a novel alginate-polyvinyl alcohol-hydroxyapatite hydrogel for 3D bioprinting bone tissue engineered scaffolds. J Biomed Mater Res A 2017;105:1457-1468.
24. Schuurman W, Khristov V, Pot MW, van Weeren PR, Dhert WJ, Malda J. Bioprinting of hybrid tissue constructs with tailorable mechanical properties. Biofabrication 2011;3:021001.
25. Detsch R, Sarker B, Grigore A, Boccaccini AR. Alginate and gelatine blending for bone cell printing and biofabrication. In: IASTED International Conference Biomedical Engineering Innsbruck. Austria: ACTA Press 2013:451-455.
26. Gelinsky M. Biopolymer hydrogel bioinks. In: Thomas DJ, Jessop ZM, Whitaker IS (eds) 3D Bioprinting for Reconstructive Surgery. Woodhead Publishing. 2018:125-136.
27. Blaeser A, Duarte Campos DF, Puster U, Richtering W, Stevens MM, Fischer H. Controlling shear stress in 3D bioprinting is a key factor to balance printing resolution and stem cell integrity. Adv Healthc Mater 2016;5:326-333.
28. Wang W, Caetano G, Ambler WS, Blaker JJ, Frade MA, Mandal P, Diver C, Bártolo P. Enhancing the hydrophilicity and cell attachment of 3D printed PCL/graphene scaffolds for bone tissue engineering. Materials 2016;9:992-103.
29. Kroeze RJ, Knippenberg M, Helder MN. Osteogenic differentiation strategies for adipose-derived mesenchymal stem cells. Methods Mol Biol 2011;702:233-248.
30. Zamani Y, Mohammadi J, Amoabediny G, Visscher DO, Helder MN, Zandieh-Doulabi B, Klein-Nulend J. Enhanced osteogenic activity by MC3T3-E1 pre-osteoblasts on chemically surface-modified poly (ε-

caprolactone) 3D-printed scaffolds compared to RGD immobilized scaffolds. Biomed Mater 2018;14:015008.

31. Tserepi A, Gogolides E, Bourkoula A, Kanioura A, Kokkoris G, Petrou P, Kakabakos S. Plasma nano textured polymeric surfaces for controlling cell attachment and proliferation: a short review. Plasma Chem Plasma P 2016;36:107-120.
32. Chang R, Nam J, Sun W. Effects of dispensing pressure and nozzle diameter on cell survival from solid free form fabrication-based direct cell writing. Tissue Eng Part A 2008;14:41-48.
33. Nair K, Gandhi M, Khalil S, Yan KC, Marcolingo M, Barbee K, Sun W. Characterization of cell viability during bioprinting processes. Biotechnol J 2009;4:1168-1177.
34. Sarker B, Rompf J, Silva R, Lang N, Detsch R, Kaschta J, Fabry B, Boccaccini AR. Alginate-based hydrogels with improved adhesive properties for cell encapsulation. Int J Biol Macromol 2015;78:72-78.
35. Jia J, Richards DJ, Pollard S, Tan Y, Rodriguez J, Visconti RP, Trusk TC, Yost MJ, Yao H, Markwald RR, Mei Y. Engineering alginate as bioink for bioprinting. Acta Biomater 2014;10:4323-4331.
36. Gungor-Ozkerim PS, Inci I, Zhang YS, Khademhosseini A, Dokmeci MR. Bioinks for 3D bioprinting: an overview. Biomater Sci 2018;6:915-946.
37. Das RK. Harnessing cell-material interaction to control cell fate: design principle of advanced functional hydrogel materials. J Chem Sci 2017;129:1807-1816.
38. Tsukanaka M, Fujibayashi S, Otsuki B, Takemoto M, Matsuda S. Osteoinductive potential of highly purified porous β-TCP in mice. J Mater Sci Mater Med 2015;26:132.
39. Wilson JL, Najia MA, Saeed R, McDevitt TC. Alginate encapsulation parameters influence the differentiation of microencapsulated embryonic stem cell aggregates. Biotechnol Bioeng 2014;111:618-631.
40. Khatab S, Leijs MJ, van Buul GM, Haeck JC, Kops N, Bos KP, Verhaar JA, Bernsen MR, van Osch GJ. Encapsulation in alginate beads prolongs mesenchymal stem cell longevity in vivo but does not enhance their therapeutic efficacy in a murine model for osteoarthritis. Osteoarth Cart 2019;27:S425-S426.